Four Phosphonium-based Ionic Liquids. Synthesis, Characterization and Electrochemical Performance as Electrolytes for Silicon Anodes

Sanchez-Ramirez, Nedher

2022-01-27

Four phosphonium-based ionic liquids. Synthesis, characterization and electrochemical performance as electrolytes for silicon anodes

Nedher Sánchez-Ramírez[a,d], Ivonne E. Monje[a], Vitor L. Martins[a], Daniel Bélanger[b], Pedro H.C. Camargo[a,c] and Roberto M. Torresi[a].

[a]Departamento de Química Fundamental, Instituto de Química – Universidade de São Paulo, Av. Prof. Lineu Prestes 748, 05500-000, São Paulo, Brazil

[b]NanoQAM and Département de Chimie Université du Québec à Montréal, Case Postale 8888 Succursale Centre-Ville, Montréal, Québec, H3C 3P8, Canada

[c]Department of Chemistry, University of Helsinki, A.I. Virtasen Aukio 1, 00014 Helsinki, Finland

[d]Departamento de Ciencias, Universidad de Ingenieria y Tecnologia – UTEC, Barranco, Lima, Peru

Graphical abstract
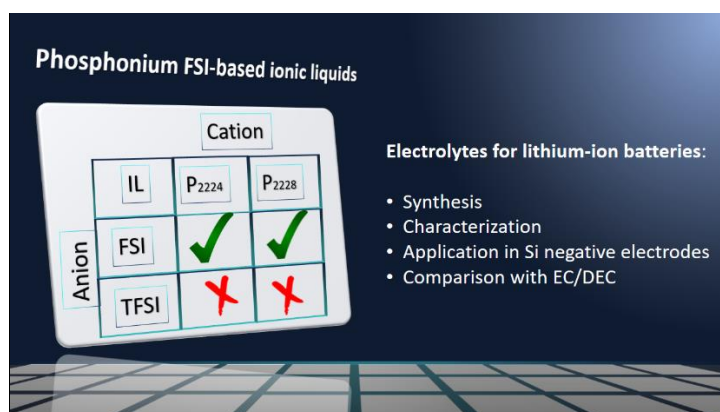
Abstract

We describe herein the synthesis, characterization and electrochemical performance as electrolyte of four phosphonium-based ionic liquids (ILs), namely: triethyl-n-butylphosphonium bis(fluoromethylsulfonyl)imide [P$_{2224}$][FSI], triethyl-n-octylphosphonium bis(fluoro-methylsulfonyl)imide[P$_{2228}$][FSI], triethyl-n-butylphosphonium bis(trifluoromethylsulfonyl)imide [P$_{2224}$][TFSI] and triethyl-n-octylphosphonium bis(trifluoromethylsulfonyl)imide [P$_{2228}$][TFSI]. Physicochemical properties such as viscosity, density, ionic conductivity, and thermal stability of ILs and conventional organic solvent, ethylene carbonate (EC)/diethly carbonate (DEC), were experimentally determined at different temperatures. All ILs showed thermal stability superior to 300 ºC, surpassing in stability the conventional organic solvent, whose flash points are 145 and 23 °C for EC and DEC, respectively. At room temperature [P$_{2224}$][FSI] is 38% less viscous than [P$_{2228}$][FSI] and the latter is 13% less viscous than [P$_{2228}$][TFSI], similarly, all ILs are much more viscous than EC/DEC. The composite Si-[P$_{2224}$][FSI] and Si-EC/DEC anodes exhibit initial specific capacities at 0.15 A/g of 2409 and 2631 mAh/g, respectively, while for those using [P$_{2228}$][FSI] and [P$_{2228}$][TFSI], the obtained charge values are found to be 1598 and 424 mAh/g. This demonstrates that despite the inferior transport properties of ILs, short-alkyl substituted phosphoniums ILs are

potentially competitive for the new generation of electrolyte for LIBs. Besides, the superior performance with FSI anions compared to TFSI was evidenced.

1. Introduction
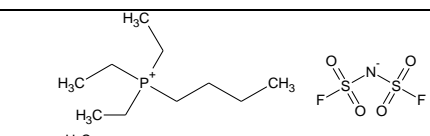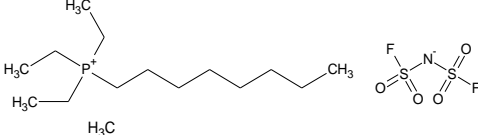
Ionic liquids (ILs) are versatile compounds that have gained considerable attention in recent years [1]. This growing interest is based on the unique and tunable properties that these substances possess, which include negligible vapor pressure, non-flammability and thermal and chemical stability, intrinsic ion conductivity, ability to dissolve a wide range of compounds, among others [2–4]. This has promoted the applications in different areas such as processing of biomass [1,5], synthesis of organic and inorganic materials [6], reagents for CO_2 capture [7], lubricant additives [8], separation-extraction agent [9]. Another promising area for ionic ILs is for electrochemical energy conversion and storage, as electrolyte for solar cells [10], electrochemical capacitors [11] and lithium ion batteries (LIBs) [4]. Regarding to this last application, the need to improve critical safety issues in LIBs besides attempts to stabilize the solid electrolyte interphase (SEI) in silicon negative electrodes has led to its recent surge [12].
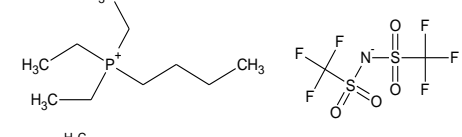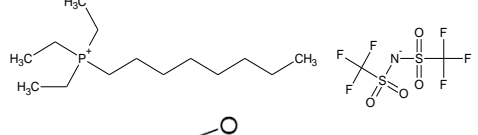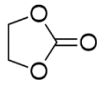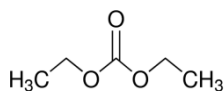
To date, conventional electrolytes are mostly based on a mixture of highly volatile and flammable alkyl carbonates solvents with lithium hexafluorophosphate ($LiPF_6$) salt [13,14]. Thermal instability of the alkyl carbonates has been closely related to fire incidents and this concern has not been overcome yet despite the enormous investigations in this field [13–15]. A peculiarity of ILs is their ability to change their properties as the structure of the anion or cation that constitutes them changes [16]. Therefore, the possibility of synthesizing thermally and electrochemically stable ILs with good transport properties makes these materials interesting for LIB technology. However, one of the greatest challenges of researchers is to synthesize ILs with low viscosity [17]. High viscosity values hinder the ion transport limiting some electrochemical applications like batteries, solar cells, or electrochemical capacitors. As all the properties of ILs, viscosity varies with different combinations of cations and anions [18], since its depends on intermolecular forces like van der Waals forces, hydrogen bonding, and Coulombic forces [19–21]. Similarly, the ionic conductivity of a solvent is fundamental in its selection for any electrochemical application [9], mainly because the performance of these devices is strongly dependent on the rate of transport or diffusion of the electroactive species to and from the electrode [20,22]. Others properties such as melting points (T_m), and thermal decomposition (T_d) temperatures are required to establish the feasible temperature operating range for any electrolyte [23]. Likewise, density data can be considered relevant for the development of equations of state involving ILs [24] and for the development of electrochemical applications where weight issues and equipment sizing are a concern [21,23].

In this context, it is essential to study the effect of the alkyl chain length of the phosphonium cations on their physicochemical properties and its effect on the electrochemical performance when using them as electrolytes. As has been shown previously, by setting the phosphonium cation, using [P2225] (triethyl-n- penylphosphonium), a comparison among TFSI (bis(trifluoromethylsulfonyl)imide) and FSI (bis(fluoromethylsulfonyl)imide) showed up to 50% higher ionic conductivity and 19% lower viscosity in FSI-based ILs [16]. In their subsequent

application as electrolytes with Si anodes, FSI-based ILs, showed a superior electrochemical performance compared to those TFSI-based, which as attributed to the stabilized SEI layer [25–27]. However, despite the fact of such interesting previous works, scarce information has been recounted on the ILs synthesized in this work and their performance with the silicon anode. Here, we report a synthesis, complete characterization, and application in Si anodes of four ILs phosphonium-based with FSI and TFSI anions used as electrolytes. Table 1 specifies the cations and anions used in this work. In addition, an analysis of the properties as the function of lithium salt concentration and comparison with commercial alkyl carbonates is showed. The results indicate that the properties of the ILs vary as the anion or cation is changed and by making an appropriate selection of them, the properties can be optimized for a specific application, as in the present work, as electrolyte with silicon anodes.

Table 1. List of phosphonium based ILs and commercial alkyl carbonates used in this work.

Compound	Structure	Abbreviation
Triethyl-n- butylphosphonium bis(fluoromethylsulfonyl)imide		$[P_{2224}][FSI]$
Triethyl-n- octylphosphonium bis(fluoromethylsulfonyl)imide		$[P_{2228}][FSI]$
Triethyl-n- butylphosphonium bis(trifluoromethylsulfonyl)imide		$[P_{2224}][TFSI]$
Triethyl-n- octylphosphonium bis(trifluoromethylsulfonyl)imide		$[P_{2228}][TFSI]$
Ethylene carbonate		EC
Diethyl carbonate		DEC

2. EXPERIMENTAL SECTION

2.1. Materials.

LiTFSI was obtained from Solvay, LiFSI, triethylphosphine, 1-bromobutane, 1-bromooctane, polyacrylonitrile (PAN, MW = 150,000 g mol^{-1}), silicon powder (size < 100 nm, <3% oxygen passivation), N,N-dimethylformamide (DMF, 99%), ethylene carbonate (EC), diethyl carbonate (DEC) and 1 molL^{-1} LiPF$_6$ in EC/DEC (battery grade) (1:1 by vol.) were used as received from the supplier (Sigma-Aldrich). For battery assembling the ILs were dried under vacuum at optimal temperature for several days until the amount of water was under 10 ppm. The moisture content of all the electrolytes studied here was determined via Karl-Fisher coulometric titration (Metrohm).

2.2. Electrode preparation

The Si/PAN electrodes were prepared according to a previously reported procedure [25,28]. 140 mg of Si nanoparticles and 60 mg of PAN were mixed in a mortar and transferred to a 5 mL beaker that contained 1.5 mL of DMF. The mixture was vigorously magnetic stirred at room temperature for 18 h. Subsequently, the electrode slurry was cast onto a copper foil current collector using a Dr. Blade with a wet film thickness of 120 μm, and then, dried in vacuum at 80 °C for 3 h. The foil was punched into 16 mm-diameter disk and the mass loading of electrode active material was 0.5-0.7 mg (0.25-0.35 mg/cm^2). The electrodes were heat-treated at 300 °C for 12 h in argon atmosphere to obtain the cyclized PAN [25,28]. All electrodes were stored under argon and not exposure to air prior assembling the half-cell batteries.

2.3. ILs Syntheses

The [P$_{2224}$][FSI], [P$_{2228}$][FSI], [P$_{2228}$][TFSI], and [P$_{2224}$][TFSI] ILs were synthesized as described elsewhere [16,29]. In a flask, 0.03 mol of P$_{2224}$Br or P$_{2228}$Br was dissolved in 50 mL of water followed by 50 mL of an aqueous solution containing LiTFSI or LiFSI (0.03 mol). The mixture was stirred for 3 hours at room temperature, the resultant IL is immiscible in water and was separated using dichloromethane. The phase containing the IL was washed several times with water, treated with activated carbon, and run through a chromatography column (alumina, dichloromethane). The IL was dried under vacuum at 45 °C for FSI based ILs and 100 °C for TFSI ILs. The characterization of the ILs by NMR and elemental analysis can be found in Figures S1-S4.

2.4 Thermal properties, density, and transport properties

Thermogravimetric analysis was carried out with a thermogravimetric analyzer (TA Instruments TGA Q500). Samples were placed in a Pt pan and heated from 25 to 700 °C with a temperature ramp of 10 °C·min^{-1}, under a flowing nitrogen atmosphere.

Differential scanning calorimetry (DSC) was carried out under a nitrogen atmosphere using a Q10 DSC system from TA Instruments with a RCS90 refrigerated cooling system and interfaced to the Advantage/Universal Analysis software. The samples for DSC measurements were sealed in a standard hermetic aluminum pan. First, the samples were cooled (10 °C min^{-1}) to −80 °C and then heated at a rate of 10 °C min^{-1} back up to 25 °C or higher. Density and viscosity were measured with a viscometer-densimeter SVM 3000 (Anton Paar) at atmospheric pressure in a temperature range of 25 to 100 °C. The ionic conductivity was determined by electrochemical impedance spectroscopy (EIS) of two parallel Pt electrodes with an Autolab PGSTAT30 in the frequency range of 10000-0.1 Hz in the range of temperature from 25 to 75 °C. The cell constant was determined with a standard KCl solution.

2.5 Galvanostatic charge/discharge

Electrochemical measurements were registered in a BioLogic BCS 805 battery tester using CR2032-type coin cells assembled in an argon-filled glovebox. The half-cell was fabricated with Si composite electrodes as working electrode and lithium metal foil as the counter electrode. Glass

micro-fiber disk (Whatman GF/F) was used as separator for $[P_{2224}][FSI]$ (1.0 molL^{-1} LiFSI), and $[P_{2228}]]FSI]$ (1.0 molL^{-1}LiFSI). Celgard-2320 was used as a separator in the case of the organic electrolyte (1.0 molL^{-1} LiPF$_6$) in EC/DEC (1:1 by vol.)], and [TFSI]-based ILs.

The half-cells were discharged (lithiated) and charged (delithiated) in a constant current testing scheme at 150 mA g^{-1} between 0.05 and 1 V (versus Li/Li$^+$). The specific capacities and current rates are given per mass of Si-active material in each composite electrode. The Coulombic efficiencies were calculated as ((Cdealloy)/(Calloy)) x 100, where Calloy and Cdealloy are the capacity of the anode for lithiation and delithiation, respectively.

3. RESULTS AND DISCUSSION

3.1. Thermal stability and melting point

Dynamic TGA

Figure 1a shows a characteristic first derivative of the TGA curve for the decomposition of the ILs. In general, ILs are considered thermally stable [29,30]; therefore, the first event upon heating corresponds to their thermal decomposition [39]. The decomposition temperature (T$_d$) was determined using the maximum of the derivative of weight loss as a reference; the T$_d$ values obtained from these experiments are listed in Table 2. The decomposition trend of all the samples considered was similar except for EC/DEC. For EC/DEC, there are two events, the weight of the sample decreased very soon at 39 °C and continues decreasing significantly at 118 °C. This fact highlights the risk of using organic solvents as electrolytes in lithium-ion batteries. Since the flashpoint EC and DEC are 145 and 23 °C, respectively [31], any abuse, including discarding in places of high temperatures, overcharging, crushing, in combination with an oxidant and an ignition source (like external short-circuiting), can generate spontaneous exothermic reactions, leading to a fire or explosion [31–33]. Since the boiling point of EC and DEC are 243 and 126 °C, respectively, and these values are higher than 39 and 118 °C, we hypothesize that they are not degradation temperatures and the peaks are associated with evaporation. This effect is more noticeable due to the small amount of sample used in the TGA experiment which is around 12 mg.

In terms of thermal stability, most organic cations used in ILs synthesis are stable at temperatures up to 350 °C. Therefore, by setting the cation, we can determine which anion has the worst impact on the degradation of the ILs. Additionally, in pyrolysis reactions, the more nucleophilic an anion the more effect it has on T$_d$ [9]. As is shown in table 2, the [TFSI]-based ILs are more thermally stable than the [FSI] counterpart due to higher nucleophilicity of [FSI] anion [16,34]. The results show that all the ILs studied present better thermal stability compare to EC/DEC solvent, with $[P_{2224}][TFSI]$ being the most thermally stable and $[P_{2224}][FSI]$ the least one.
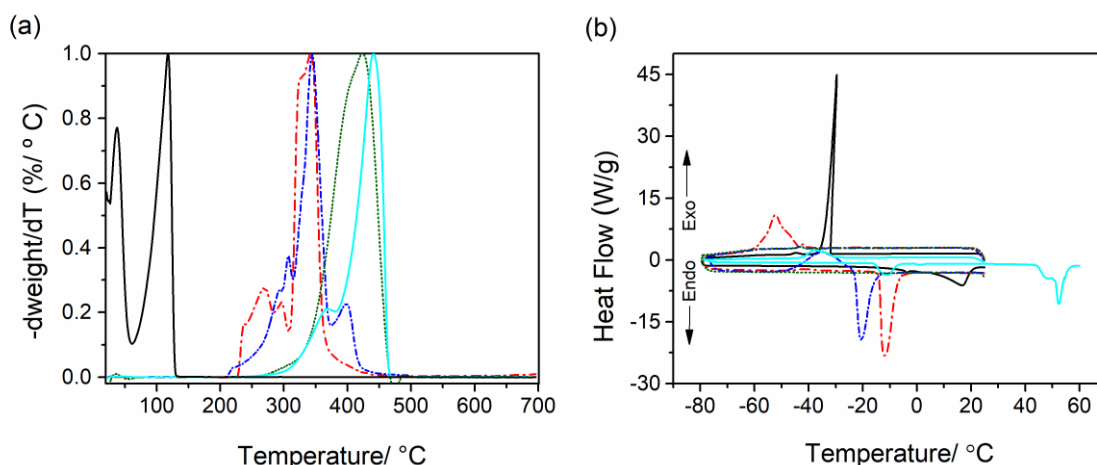
Figure 1. (a) First derivative of dynamic TGA sketch for the studied ILs and the organic solvent. (b) DSC curve for all substances (exothermic processes – up). EC/DEC, black line; [P$_{2224}$][FSI], red dash dot line; [P$_{2228}$][FSI], blue short dash dot line; [P$_{2228}$][TFSI], green short dot line; [P$_{2224}$][TFSI], cyan line.

DSC

The DSC traces of all four ILs are displayed in Figure 1b. From the figure, [P$_{2228}$][TFSI] represents the simplest case because it was in the liquid phase in all the temperature range. Conversely, [P$_{2224}$][TFSI] is solid at room temperature, the only event that appears is the melting point (T$_m$). The remaining three ILs have crystallization and fusion processes.

The T$_m$ is inversely proportional to the size of the cations [9,35]. This explains the following trend in T$_m$: [P$_{2228}$][TFSI]< [P$_{2224}$][TFSI] and [P$_{2228}$][FSI]< [P$_{2224}$][FSI]. The comparison between [FSI] and [TFSI] based ILs is hindered because it depends on the coordination capacity [36], sizes and shapes [9,35] of the anion, and the importance of each one will depend on the cation, therefore it is difficult to establish a trend.

 TGA and DSC results show that all ILs, except [P$_{2224}$][TFSI], have a large liquids range in which they could be used as electrolytes in the liquid phase without decomposition. Since [P$_{2224}$TFSI] is solid at room temperature, other measurements such as transport properties were not carried out.

3.2. Viscosity, Conductivity, and Density Measurement

Table 2 presents the viscosity at 25 °C and Figure 2a at different temperatures. The viscosity of ILs is strongly dependent on temperature. For instance, the viscosity of [P$_{2228}$][TFSI] decreases by 25% when the temperature increases from 27 to 33 °C. The increase in temperature causes an increase in the kinetic energy of the molecules causing a reduction of intermolecular or internal forces. It is noticeable that [P$_{2228}$][FSI] is 13% less viscous than [P$_{2228}$][TFSI]. This can be ascribed to the decrease of two intermolecular forces; the smaller size of [FSI] anion that decreases the van der Waals force, and to better distribution and stabilization of the negative charge in the [FSI] anion that causes lower Coulombic interactions [37–40]. From the point of view of the cation, another interesting point is that [P$_{2224}$][FSI] is 38% less viscous than [P$_{2228}$][FSI]. When the alkyl chain length increases the intermolecular forces (van der Waals and Coulombic) do likewise [41]. We can also notice that from Table 2 that all ILs are significantly more viscous than the EC/DEC solvent,

which represents the main weak point of these substances [25]. Nevertheless, when used as electrolyte with a silicon anode, FSI-based ILs can remarkably stabilize the SEI [25] compare to the organic solvent, hence can somewhat compensate for the drawback related to the transport properties.
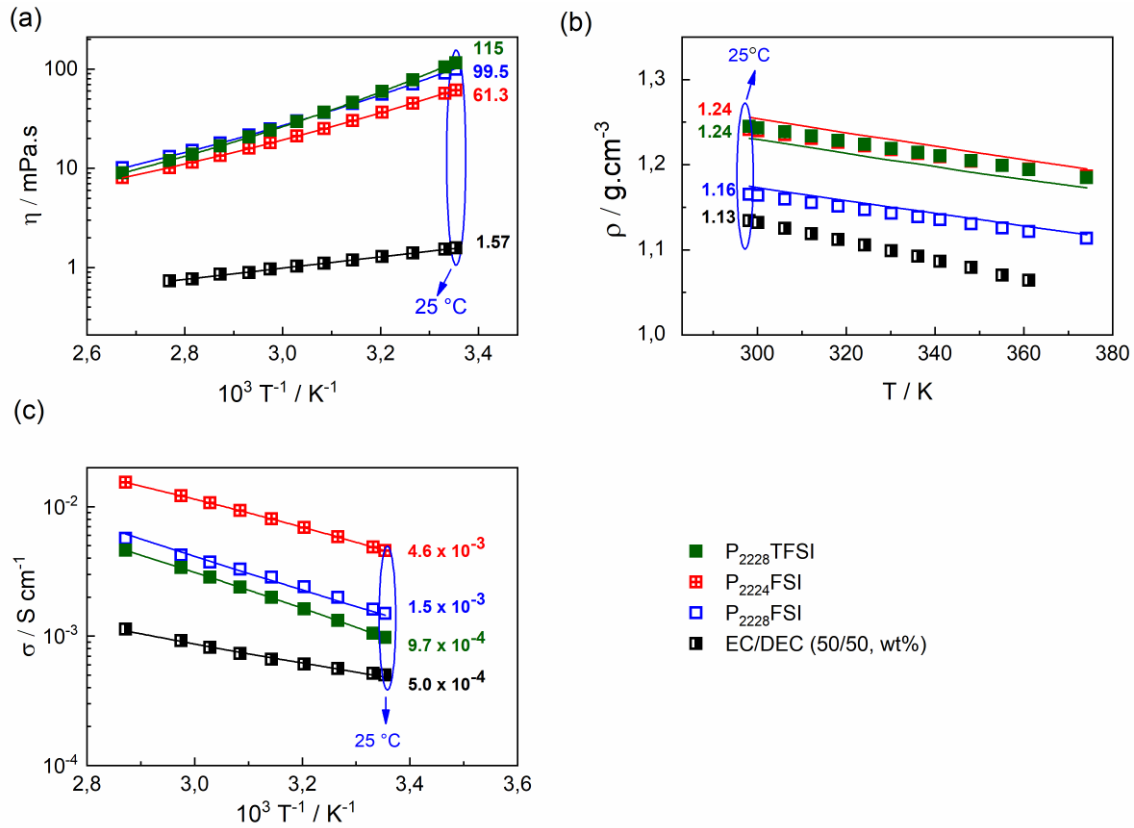
Figure 2. (a) Arrhenius plots of the viscosity of neat ILs. The lines represent the best fits of the Vogel–Tamman–Fulcher equation. (b) Density at different temperatures for neat ILs. (c) Arrhenius plot of ILs' temperature-dependent conductivity data. Lines represent the best fits of the VTF equations for viscosity and ionic conductivity and estimated density from Equation (1). [P$_{2224}$][FSI] 1M LiFSI (red plus square ⊞), [P$_{2228}$][FSI] 1M LiFSI (blue square ▫), [P$_{2228}$][TFSI] 1M LiTFSI (green filled square ■), EC/DEC (half-filled black circle ◨).

Table 2. Selected properties of the electrolytes neat ILs and organic solvent and their 1.0 mol L^{-1} Li$^+$ salt mixtures at 298.15 K.

IL	Salt concentration	η [mPa.s]	σ [mS.cm^{-1}]	ρ [g.cm^{-3}]	T_d [°C]	T_m [°C]
[P$_{2228}$][TFSI]	Pure	115	0.971	1.24	423	< -80
[P$_{2228}$][TFSI]	1.0 mol L^{-1} LiTFSI	443	0.224	1.33	-	-
[P$_{2228}$][FSI]	Pure	99.5	1.50	1.16	344	-20.6
[P$_{2228}$][FSI]	1.0 mol L^{-1} LiFSI	142	1.05	1.23	-	-
[P$_{2224}$][FSI]	pure	61.3	4.6	1.24	342	-11.9
[P$_{2224}$][FSI]	1.0 mol L^{-1}	97.3	2.52	1.31	-	-

	LiFSI					
EC/DEC(50wt%)	pure	1.57	0.498	1.13	39	16.7
EC/DEC(50wt%)	1.0 mol L^{-1} LiPF$_6$	4.7 [42]	7.8 [42]	1.2[42]	-	-
[P$_{2224}$][TFSI]	pure	-	-	-	441	52.4

Table 2 shows the ionic conductivity at 25 °C and Figure 2c at different temperatures. It can be seen that at 25 °C, [P$_{2228}$][FSI] is 35% more conductive than [P$_{2228}$][TFSI]. By other hand, the conductivity of [P$_{2224}$][FSI] was found to be 67% greater than [P$_{2228}$][FSI]. The more viscous an IL is, the less conductive it becomes [16], therefore the same explanations given for viscosity can be given for conductivity. It should be noticed that ionic conductivity is generally measured by EIS, however, its value gives a broad picture because it represents the contribution of all charged species in the IL [15,20].

Nevertheless, Table 2 indicates that when we compare [P$_{2224}$][FSI] vs. [P$_{2228}$][FSI] and [P$_{2228}$][FSI] vs. [P$_{2228}$][TFSI], the decrease of the ionic conductivity cannot be completely attributed to the detrimental effect of the viscosity. Walden plot will allow to give a better explanation of this aspect. Walden plot is a log-log chart of molar conductivity (S.mol^{-1}.cm^2) vs. 1/viscosity (poise^{-1}), which indicates the number of mobile charge carriers in an IL (ionicity). Data are compared to the "ideal case" of 0.01 M KCl or LiCl which exists as a dissociated ion and represented as a dotted line in Figure 3 [9,43]. Data points that are higher than the "ideal" line belonging to the region known as superionic indicate a decoupling of the ion transport from the macroscopic viscosity. Values that are below the "ideal" belonging to the subionic region regime indicate that there are many ion pairs in the electrolyte that do not contribute to the overall conductivity [44][45]. Thus, from Figure 3a, it can be seen that TFSI (compared to FSI anion and using P$_{2228}$ as a cation) facilitates in a higher degree the formation of aggregates that decrease the electrochemical conductivity of ILs. In an experiment with lithium cations, the TFSI anion has been previously reported to have shorter interactions due to their superior coordination capacity compared to the FSI anion [40].

When comparing [P$_{2228}$][FSI] with [P$_{2224}$][FSI], it can be seen that the former is closer to the ideal line, this indicates the existence of tight ion pairs that do not undergo significant dissociation under the influence of an electric field and, therefore, do not contribute to the ionic conductivity [46]. The explanation is that van der Waals interaction increases with the alkyl side chain [41,47]. Additionally, it has been reported that ILs having an alkyl chain length of 8 C-atoms or more markedly increase the formation of aggregates [48].

The ILs densities appear to be the least sensitive physical property to variation in temperature regardless of the ionic liquid structures [9,49]. For example, a 6 °C change in temperature from 27 to 33 °C results in only a 0.4 % decrease in the density for [P$_{2224}$][FSI], the same trend is observed for [P$_{2228}$][TFSI]. Table 2 presents the densities at 25 °C and Figure 2b at different temperatures. Since the molar mass of [TFSI] and [FSI] are 280.1 and 180.1 gmol^{-1}, respectively, from the table it is possible to deduce that the density of the ILs is proportional to the molar mass of the anion: [P$_{2228}$][FSI] < [P$_{2228}$][TFSI]. This trend is due to the nature of the anions under study. Heavier

anions, except for those with high steric effect, can occupy favorable, relatively close-approach positions around the cation, resulting in high densities [16,23]. The effect of the alkyl chain can also be seen in Table 2. [P$_{2228}$][FSI] is less dense than [P$_{2224}$][FSI]. As the length of the chain increases, the cation becomes more asymmetric, leading to more difficult packing [8,16,23]. Finally, unlike viscosity, the density of ILs is very similar to the density of conventional EC/DEC.

3.3 Viscosity, conductivity and density estimation

For many ILs, as is the case of the liquids reported in this investigation, the temperature dependence of η is often well described by the Vogel–Tamman–Fulcher (VTF) equation in a broad temperature range above Tg [51]. This equation is commonly used to quantify the deviation from Arrhenius behavior for glass-forming materials near Tg. Although the Arrhenius model was originally used to describe how the kinetic constants in chemical reactions vary with temperature [52], this model appears to be a framework for describing the temperature dependence of transport properties such as viscosity and conductivity [53].

To describe the deviation of the Arrhenius model some parameters are introduced, thus, the change in viscosity with temperature is analyzed using the general VTF equation [54]:

$$\eta = \eta_o exp\left(\frac{B}{T-T_0}\right) = \eta_o exp\left(\frac{DT_0}{T-T_0}\right) \qquad (1)$$

where B is a fitting parameter, and T_0 is the ideal glass transition temperature. The parameter D (B/T_0) used in the alternative form of the equation (1) describes the "strength" or fragility of a liquid. The fragility concept can be utilized to categorize liquids for their temperature-dependent viscosity, strong liquids (large D) have a very low variability [53]. Table S1 shows the VTF parameters obtained for all electrolytes in the analyzed temperature range.

Similarly, as viscosity, the conductivity is often best described using the empirical VTF equation [25,55]:

$$\sigma = \sigma_o exp\left(\frac{-B'}{T-T_0'}\right) \qquad (2)$$

where σ$_o$, B', and T$_o$ are the adjustable parameters, which can be seen in Table S2.

To calculate the theoretical density of an IL, Coutinho et al. [56] have modified the Ye and Shreeve equation [57] and proposed the following formula:

$$\rho_{cal.} = \frac{M(gmol^{-1})}{N.V(Å^3)[a+b\cdot T(K)]+c\cdot p(MPa)]} 10^{24}\left(Å^3 cm^{-3}\right) \quad (3)$$

where a, b and c are the correction factors 0.8005, 6.652 x 10^{-4} K^{-1}, and -5.919 x 10^{-4} MPa^{-1}, respectively. M is the molecular weight (g mol^{-1}), T is the temperature (K), p is the pressure (MPa) and V (Å^3) is the linear sum of the cation and anion volumes. The following volume were used in equation (3), 443 Å^3 for [P$_{2228}$] [30,57], 331 Å^3 for [P$_{2224}$] [30,57], 248 Å^3 for [TFSI] [57,58] and 139.7 Å^3 for [FSI][59].

Table 3. Calculated and experimental density for the neat ILs at 298 and 373 K.

IL	Temperature	$\rho_{exp.}$ (g cm^{-3})	$\rho_{calc.}$ (g cm^{-3})	|Error (%)|*
[P$_{2228}$][TFSI]	298	1.245	1.231	1.12
	373	1.185	1.173	1.01
[P$_{2228}$][FSI]	298	1.165	1.175	0.85
	373	1.113	1.118	0.45
[P$_{2224}$][FSI]	298	1.241	1.256	1.21
	373	1.187	1.195	0.67

*Calculated as the difference between $\rho_{exp.}$ and $\rho_{calc.}$, divided by the $\rho_{exp.}$, multiplied by 100.

Table 3 summarizes the experimental density and the calculated density at 298 K and 373 K for the neat ILs. It can be noted that unlike the [P$_{2228}$][TFSI], the ILs derived from FSI present a $\rho_{calc.}$ slightly higher than the $\rho_{exp.}$ This could be due the fact that the FSI anion has a lower coordination capacity compared to the TFSI anion, FSI-based liquids have higher free volume, leading to experimental densities lower than those estimated with equation (3) who considers separate building blocks that do not interact with each other [29,57]. A similar trend was observed comparing the experimental and calculated densities of the ILs derived from [B(CN)$_4$] and [TFSI] [29].

Since the free volume increases linearly with temperature [60], it is expected that as the temperature increases, the anions and cations of the IL have more freedom to move, therefore their behavior is more similar to that predicted by equation (3), this explains why in all cases at 378 K the % error decreases. In table 3 the error percentages for the density of the ILs and their Li$^+$ mixtures are reported. As explained below, the presence of lithium salt causes new interactions between the ions, since these are not considered in equation 3, consequently, the % error increases.

3.4 ILs with lithium salt 1 mol L^{-1}

The same trend for neat ILs can be observed when we analyze the same electrolytes with a 1 mol L^{-1} lithium salt (Figure 3b). Nevertheless, electrolytes are even lower than the ideal line than when they are pure, the dissolution of the [Li$^+$][X$^-$] salt in the [A$^+$][X$^-$] ionic liquid leads to a ternary system [Li$^+$]$_m$[A$^+$]$_n$[X$^-$]$_{(m+n)}$ with increased viscosity and lower conductivity provoked by the formation of large aggregates due to the presence of lithium salt [61,62]. This explains why the viscosity and density increase and the conductivity decreases for all liquids reported in Table 2 and Figure 4. As in the case of pure liquids, this effect is more pronounced for the cation [P$_{2228}$] and the anion [TFSI].

For EC/DEC organic solvent, there is also a departure from the ideal line when a lithium salt is added. However, this effect is less noticeable for the organic solvent, due to the concentration of 1 mol L^{-1} of lithium salt; there is an increase in viscosity (66%) but there is an increase in conductivity (93%). On the other hand, for ILs, the addition of lithium salt causes detrimental effects on both properties. Figure 4 displays the density and transport properties for all ILs using 1M lithium salt. As in Figure 3b, in Figure 4 for organic solvent, only the data at 25 °C is shown.
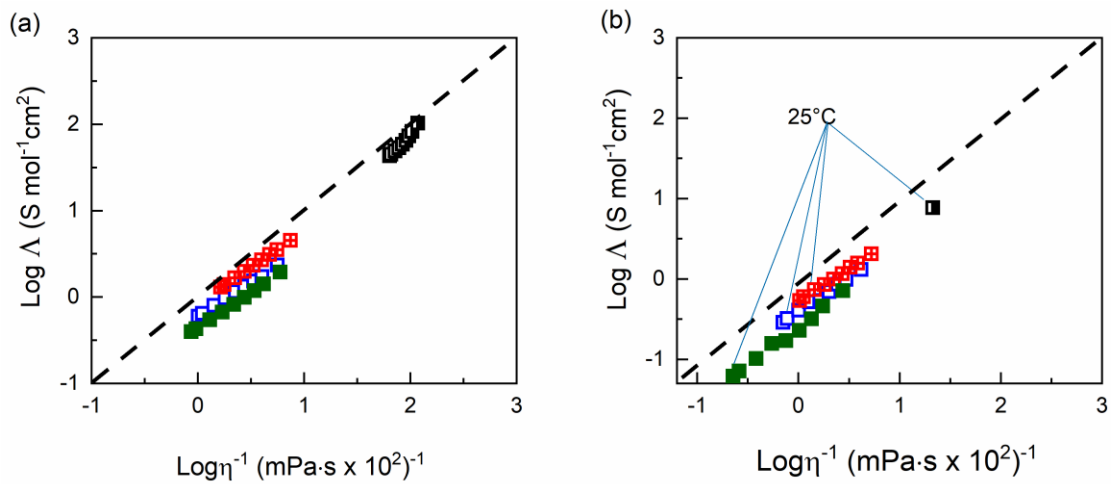
Figure 3. Walden plot (log−log) of (a) neat ILs, [P$_{2224}$][FSI] 1M LiFSI (red plus square ⊞), [P$_{2228}$][FSI] 1M LiFSI (blue square ☐), [P$_{2228}$][TFSI] (green filled square ■), EC/DEC (half-filled black circle ◨). (b) 1M LiFSI for [P$_{2224}$][FSI] and [P$_{2228}$][FSI], 1M LiTFSI for [P$_{2228}$][TFSI] and 1M LiPF$_6$ for EC/DEC.
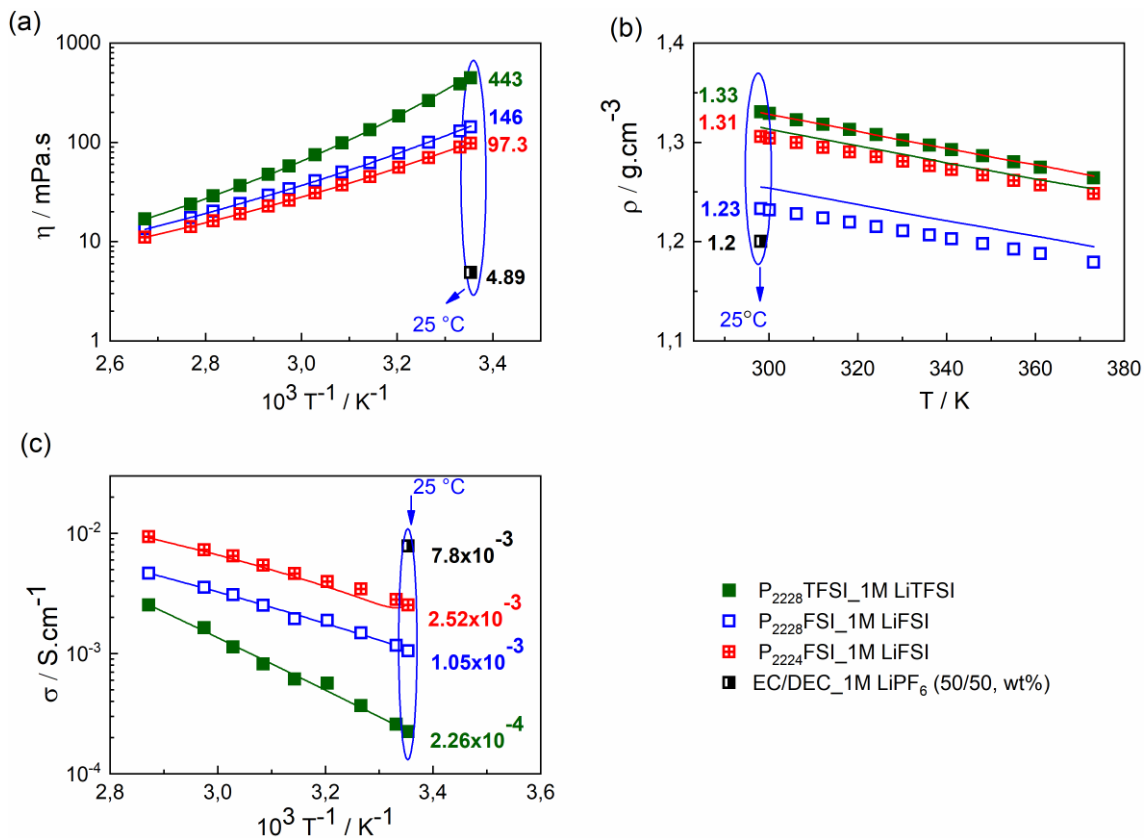
Figure 4. Effect of lithium salt on the density and transport properties of different electrolytes. (a) Arrhenius plots of the viscosity (b) Density at different temperatures (c) Arrhenius plot of ILs' temperature-dependent conductivity data. Lines represent the best fits of the VTF equations for viscosity and ionic conductivity and estimated density from Equation (3). [P$_{2224}$][FSI] 1M LiFSI

(red plus square ⊞), [P$_{2228}$][FSI] 1M LiFSI (blue square ☐), [P$_{2228}$][TFSI] 1M LiTFSI (green-filled square ■), EC/DEC (half-filled black circle ◓).

3.5 Ionic liquids as electrolytes with silicon negative electrodes

To evaluate the synthesized ILs as electrolytes in LIBs, a set of Si/PAN composites were galvanostatic discharge/charge with each electrolyte. Figure 5 shows some of the potential profiles between 0.05 and 2.5 V cutoff of the four composites electrodes that were used to obtain the data of Fig. 5b. The voltage profiles correspond to the first, second, and 30 cycles at 150 mAh/g. The first charge shows the characteristic profile of the lithiation of crystalline silicon particles. During lithiation in all four electrolytes, a long flat voltage plateau at ca. 0.08 V, suggest both the LixSi alloy formation from crystalline silicon with lithium reaction and reduction of electrolyte to form the SEI layer[25,63,64]. In the subsequent charge process, decomposition of LixSi and the extraction of Li ions from the lithiated silicon host take place[65].

The composite electrode with EC/DEC delivers a delithiation capacity of 2631 mAh/g, while for [P$_{2224}$][FSI] 1 mol L^{-1} LiFSI; [P$_{2228}$][FSI] 1 mol L^{-1} LiFSI and [P$_{2228}$][TFSI] 1 mol L^{-1} LiTFSI, the obtained charge values are found to be 2409, 1598 and 424 mAh/g. The average delithiation capacity is slightly superior for EC/DEC compared to [P$_{2224}$][FSI] (~9%), while it is considerably lower for ILs in which [P$_{2228}$] cations were used. In the second cycle, slight improvements in the delithiation capacity in all samples (10-12%) may suggest the formation of a more stable SEI layer. From cycle 5 to 30, the current density varied in the range of 500 to 2000 mA/g, it can be observed that as the current increases, which implies less time for the lithiation and delithiation process, the capacity decreases in greater proportion for the ILs compared to the organic solvent. This can be ascribed to the fact that the latter has better transport properties. On the other hand, analyzing all the current densities in figure 5b, [P$_{2224}$][FSI] (1.0 M LiFSI) electrolyte yielded an average Coulombic efficiency of 98.4 %. Furthermore, [P$_{2228}$][FSI] (1.0 M LiFSI) and EC/DEC (1M LiPF$_6$) exhibited Coulombic efficiencies of 98.2 and 97.5%, respectively.

In general, the observed delithiation trend matches those values obtained for ionic conductivity and are inverse to viscosity (Figure 4). Remarkably, the fact that similar capacities are obtained for EC/DEC and [P$_{2224}$][FSI] and that the latter present a higher Coulombic efficiency, evidence that in spite of the inferior transport properties of ILs, short-alkyl substituted phosphonium ILs can be plausible use as electrolytes. However, to analyze the SEI layer in more extreme conditions further studies to evaluate both the behavior of half-cells at different rates (150 to 1000 mAg^{-1}) and during long cycling are needed, the ILs based on FSI have shown to be promising in this regard [25].
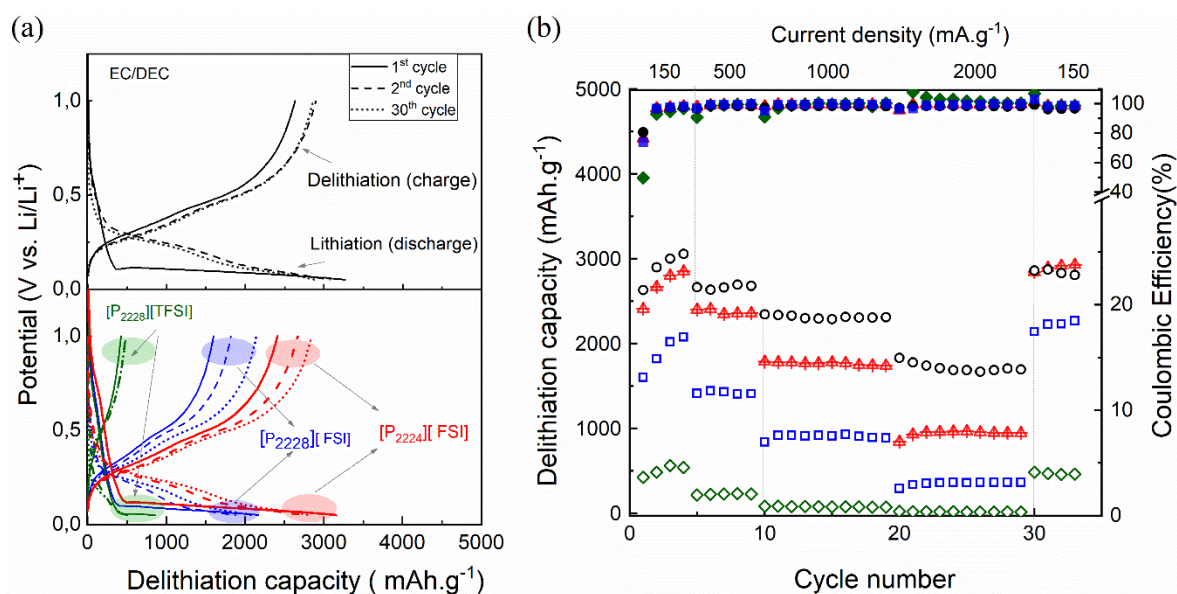
Figure 5. Discharge/charge voltage profile of the first, second, and 30th cycles at 150 mAg^{-1} for Si/PAN electrodes in different electrolytes (a). 1st cycle, line; 2nd cycle dash-dot line, and 30th cycle continuous line. (Top) EC/DEC 1 molL^{-1} LiPF$_6$ (black) and (Bottom) ILs. [P$_{2224}$][FSI] 1 molL^{-1} LiFSI (red); [P$_{2228}$][FSI] 1 molL^{-1} LiFSI (blue); and [P$_{2228}$][TFSI] 1 molL^{-1} LiTFSI (green). Cut-off potentials were 1 and 0.05 V. Specific delithiation capacities, unshaded simbols; and Coulombic efficiency, shaded simbols of the electrodes shown in (a) are shown in (b). EC/DEC 1 molL^{-1} LiPF$_6$ (black circles○) and ILs. [P$_{2224}$][FSI] 1 molL^{-1} LiFSI (red triangles ▲); [P$_{2228}$][FSI] 1 molL^{-1} LiFSI (blue squares □); and [P$_{2228}$][TFSI] 1 molL^{-1} LiTFSI (green diamonds ◇).

4. CONCLUSIONS

The properties for four ILs derived from phosphonium were measured: [P$_{2224}$][FSI], [P$_{2228}$][FSI] [P$_{2228}$][TFSI] and [P$_{2224}$][TFSI]. All neat ionic liquids showed thermal stability superior to 300 ℃, surpassing in terms of stability the conventional organic solvent, whose flask points are 145 and 23 ℃ for EC and DEC, respectively. At room temperature [P$_{2224}$][FSI] is 38% less viscous than [P$_{2228}$][FSI] and the latter is 13 % less viscous than [P$_{2228}$][TFSI]. All ILs are much more viscous than EC/DEC. The addition of lithium salt increases the viscosity of all substances and does not change this trend. At room temperature the conductivity of [P$_{2224}$][FSI] was found to be 67% greater than [P$_{2228}$][FSI] and [P$_{2228}$][FSI] is 34% more conductive than [P$_{2228}$][TFSI]. Similarly to the viscosity, the addition of lithium salt worsens the conductivity for ILs, conversely to the observed for organic solvent electrolyte, which was attributed to the formation of agglomerates that decrease the mobility of the ions. The Walden plot showed higher ionicity for [P$_{2224}$][FSI] compared to the other ILs, which gives it an advantage as an electrolyte. An additional conclusion is that [P$_{2224}$][TFSI] cannot be used as an electrolyte since it is solid at RT. Finally, it is remarkable that the composite Si anode with [P$_{2224}$][FSI] IL and EC/DEC exhibit initial specific capacities, at 0.15A/g, of 2409 and 2631 mAh/g, respectively. This demonstrates that despite the inferior transport properties of ILs, short-alkyl substituted phosphonium ILs can be potentially used as electrolytes. However, more studies at higher rates and long cycling are needed. To sum, all liquids

showed electrochemical stability in the lithium alloying potential window and are recommended as electrolytes in studies of lithium-ion batteries, involving the promising above-mentioned anode.

Funding

Notes

The authors declare no competing financial interest.

References

[1]   Welton T. Ionic liquids: a brief history. Biophys Rev 2018;10:691–706.

[2]   Bazito FFC, Kawano Y, Torresi RM. Synthesis and characterization of two ionic liquids with emphasis on their chemical stability towards metallic lithium. Electrochim Acta 2007;52:6427–37.

[3]   MacFarlane DR, Forsyth M, Howlett PC, Kar M, Passerini S, Pringle JM, et al. Ionic liquids and their solid-state analogues as materials for energy generation and storage. Nat Rev Mater 2016:1–15.

[4]   MacFarlane DR, Tachikawa N, Forsyth M, Pringle JM, Howlett PC, Elliott GD, et al. Energy applications of ionic liquids. Energy Environ Sci 2014;7:232–50.

[5]   Kilpeläinen Il, Xie Ha, King Al, Granstrom M, Heikkinen S, Argyropoulos D. Dissolution of Wood in Ionic Liquids. J Agric Food Chem 2007;55:9142–8.

[6]   Freemantle M. Introduction to Ionic Liquids. Cambridge: firts ed., RCS publishing; 2010.

[7]   Blanchard L, Hancu D, Beckman E, Brennecke JF. Green processing using ionic liquids and CO2. Nature 1999;399:28–9.

[8]   Zhou Y, Qu J. Ionic Liquids as Lubricant Additives : A Review. ACS Appl Mater Interfaces 2017;9:3209–22.

[9]   Wasserscheid P, Welton T. Ionic Liquid in Synthesis. second ed. Weinheim, Germany: Wiley-VCH; 2008.

[10]   Kuang D, Wang P, Ito S, Zakeeruddin SM, Grätzel M. Stable mesoscopic dye-sensitized solar cells based on tetracyanoborate ionic liquid electrolyte. J Am Chem Soc 2006;128:7732–3.

[11]   Rennie AJR, Sanchez-Ramirez N, Torresi RM, Hall PJ. Ether-bond-containing ionic liquids as supercapacitor electrolytes. J Phys Chem Lett 2013;4:2970–4.

[12]   Martins VL, Neves HR, Monje IE, Leite MM, De Oliveira PFM, Antoniassi RM, et al. An overview on the development of electrochemical capacitors and batteries – part ii. An Acad Bras Cienc 2020;92:1–29.

[13] Chawla N, Bharti N, Singh S. Recent advances in non-flammable electrolytes for safer lithium-ion batteries. Batteries 2019;5:1–25.

[14] Wang J, Yamada Y, Sodeyama K, Watanabe E, Takada K, Tateyama Y, et al. Fire-extinguishing organic electrolytes for safe batteries. Nat Energy 2018;3:22–9.

[15] Ohno H. Electrochemical Aspects of Ionic Liquids. 1st ed. Hoboken: John Wiley & Sons; 2011.

[16] Sanchez-Ramírez N, Desalegn Assresahegn B, Bélanger D, Torresi RM. A Comparison among Viscosity, Density, Conductivity, and Electrochemical Windows of N-n-Butyl-N-methylpyrrolidinium and Triethyl-n-pentylphosphonium Bis(fluorosulfonyl imide) Ionic Liquids and Their Analogues Containing Bis(trifluoromethylsulfonyl) Imide . J Chem Eng Data 2017;62:3437–44.

[17] Martins VL, Torresi RM. Ionic liquids in electrochemical energy storage. Curr Opin Electrochem 2018;9:26–32.

[18] Koi ZK, Zaireen W, Asykin R, Kiki Adi K. Prediction of the viscosity of imidazolium-based ionic liquids at different temperatures using the. New J Chem 2019;43:16207–17.

[19] Barthen P, Frank W, Ignatiev N. Development of low viscous ionic liquids : the dependence of the viscosity on the mass of the ions. Ionics (Kiel) 2015;21:149–59.

[20] Macfarlane D, Kar M, Pringle JM. Fundamentals of Ionic Liquids: From Chemistry to Applications. 1st ed. Hoboken: John Wiley & Sons; 2017.

[21] O'Mahony AM, Silvester DS, Aldous L, Hardacre C, Compton RG. Effect of water on the electrochemical window and potential limits of room-temperature ionic liquids. J Chem Eng Data 2008;53:2884–91.

[22] Hirayama H, Tachikawa N, Yoshii K, Watanabe M, Katayama Y. Electrochemistry 2015;83:824–7.

[23] Fredlake CP, Crosthwaite JM, Hert DG, N. V. K.Aki S, Brennecke JF. Thermophysical Properties of Imidazolium-Based Ionic Liquids. J Chem Eng Data 2004;49:954–64.

[24] Santos D, Santos M, Franceschi E, Barison A. Experimental Density of Ionic Liquids and Thermodynamic Modeling with Experimental Density of Ionic Liquids and Thermodynamic Modeling with Group Contribution Equation of State Based on the Lattice Fluid Theory. J Chem Eng Data 2015;61:348–53.

[25] Sanchez-Ramirez N, Assresahegn BD, Torresi RM, Bélanger D. Producing high-performing silicon anodes by tailoring ionic liquids as electrolytes. Energy Storage Mater 2020;25:477–86.

[26] Piper DM, Evans T, Leung K, Watkins T, Olson J, Kim SC, et al. Stable silicon-ionic liquid interface for next-generation lithium-ion batteries. Nat Commun 2015;6:6:6230.

[27] Kerr R, Mazouzi D, Eftekharnia M, Lestriez B, Dupré N, Forsyth M, et al. High-Capacity Retention of Si Anodes Using a Mixed Lithium/Phosphonium Bis(fluorosulfonyl)imide Ionic Liquid Electrolyte. ACS Energy Lett 2017;2:1804–9.

[28] Piper DM, Yersak TA, Son SB, Kim SC, Kang CS, Oh KH, et al. Conformal coatings of

cyclized-PAN for mechanically resilient Si nano-composite anodes. Adv Energy Mater 2013;3:697–702.

[29]   Sanchez-Ramirez N, Martins VL, Ando R, Camilo F, Urahata S, Ribeiro MCC, et al. Physicochemical Properties of Three Ionic Liquids Containing Tetracyanoborate Anion and Their Lithium Salt Mixtures. J Phys Chem B 2014;118:8772–8781.

[30]   Martins VL, Sanchez-Ramirez N, Ribeiro MCC, Torresi RM. Two phosphonium ionic liquids with high Li+ transport number. Phys Chem Chem Phys 2015;17:23041–51.

[31]   Hess S, Wohlfahrt-Mehrens M, Wachtler M. Flammability of Li-ion battery electrolytes: Flash point and self-extinguishing time measurements. J Electrochem Soc 2015;162:3084–97.

[32]   Balakrishnan PG, Ramesh R, Prem Kumar T. Safety mechanisms in lithium-ion batteries. J Power Sources 2006;155:401–14.

[33]   Jeevarajan JA, Winchester CS. Battery Safety Qualifications for Human Ratings. Interface-Electrochemical Soc 2012;21:51–5.

[34]   Beyersdorff T, Schubert TJS, Welz-Biermann U, Pitner W, Abbott AP, McKenzie KJ, et al. Synthesis of Ionic Liquids. In: Endres F, MacFarlane D, Abbott A, editors. Electrodepos. from Ion. Liq., Weinheim: Wiley-VCH Verlag GmbH & Co. KGaA; 2008, p. 15–46.

[35]   Davis, Jr. JH. Task-Specific Ionic Liquids. Chem Lett 2004;33:1072–7.

[36]   Ueno K, Tokuda H, Watanabe M. Ionicity in ionic liquids: correlation with ionic structure and physicochemical properties. Phys Chem Chem Phys 2010;12:1649–58.

[37]   Borodin O, Gorecki W, Smith GD, Armand M. Molecular dynamics simulation and pulsed-field gradient NMR studies of bis(fluorosulfonyl)imide (FSI) and bis[(trifluoromethyl)sulfonyl]imide (TFSI)-based ionic liquids. J Phys Chem B 2010;114:6786–98.

[38]   Tsuzuki S, Hayamizu K, Seki S. Origin of the low-viscosity of [emim][(FSO2)2N] ionic liquid and its lithium salt mixture: Experimental and theoretical study of self-diffusion coefficients, conductivities, and intermolecular interactions. J Phys Chem B 2010;114:16329–36.

[39]   Fujii K, Seki S, Fukuda S, Takamuku T, Kohara S, Kameda Y, et al. Liquid structure and conformation of a low-viscosity ionic liquid, N-methyl-N-propyl-pyrrolidinium bis(fluorosulfonyl) imide studied by high-energy X-ray scattering. J Mol Liq 2008;143:64–9.

[40]   Fujii K, Hamano H, Doi H, Song X, Tsuzuki S, Hayamizu K, et al. Unusual Li+ ion solvation structure in bis(fluorosulfonyl)amide based ionic liquid. J Phys Chem C 2013;117:19314–24.

[41]   Rashid T, Kait CF, Murugesan T. Effect of alkyl chain length on the thermophysical properties of pyridinium carboxylates. Chinese J Chem Eng 2016;25:1266–72.

[42]   Lundgren H, Behm M, Lindbergh G. Electrochemical Characterization and Temperature Dependency of Mass-Transport Properties of LiPF6 in EC:DEC. J Electrochem Soc 2015;162:A413–20.

[43]   Austen Angell C, Ansari Y, Zhao Z. Ionic Liquids: Past, present and future. Faraday Discuss 2012;154:9–27.

[44]   Fan F, Wang W, Holt AP, Feng H, Uhrig D, Lu X, et al. Effect of molecular weight on the ion transport mechanism in polymerized ionic liquids. Macromolecules 2016;49:4557–70.

[45]   MacFarlane DR, Forsyth M, Izgorodina EI, Abbott AP, Annat G, Fraser K. On the concept of ionicity in ionic liquids. Phys Chem Chem Phys 2009;11:4962–7.

[46]   Papović S, Gadžurić S, Bešter-Rogač M, Vraneš M. Effect of the alkyl chain length on the electrical conductivity of six (imidazolium-based ionic liquids + γ -butyrolactone) binary mixtures. J Chem Thermodyn 2016;102:367–77.

[47]   Khan MK, Sundararajan PR. Effects of Carbon Atom Parity and Alkyl Side Chain Length on the Crystallization and Morphology of Biscarbamates , A Set of Model Compounds for Polyurethanes. J Phys Chem B 2011;115:8696–706.

[48]   Goodchild I, Collier L, Millar SL, Prokeš I, Lord JCD, Butts CP, et al. Structural studies of the phase , aggregation and surface behaviour of 1-alkyl-3-methylimidazolium halide + water mixtures 2007;307:455–68.

[49]   Ohno H. Physical Properties of Ionic Liquids for Electrochemical Applications. In: Endres F, MacFarlane D, Abbott A, editors. Electrodepos. from Ion. Liq., Weinheim: Wiley-VCH Verlag GmbH & Co. KGaA; 2008.

[50]   Wassercheid P, Welton T. Ionic Liquids in Synthesis. Wiley-Weinheim; 2003.

[51]   Zheng W, Mohammed A, Hines LG, Xiao D, Martinez OJ, Bartsch RA, et al. Effect of Cation Symmetry on the Morphology and Physicochemical Properties of Imidazolium Ionic Liquids. J Phys Chem B 2011;115:6572–84.

[52]   Ferreira DC, Luiza M, Almeida OD. Difficulties in the application of the Arrhenius model to predict thermal printing lifetime 2014.

[53]   Schreiner C, Zugmann S, Hartl R, Gores HJ. Temperature dependence of viscosity and specific conductivity of fluoroborate-based ionic liquids in light of the fractional walden rule and Angell's fragility concept. J Chem Eng Data 2010;55:4372–7.

[54]   Hayamizu K, Aihara Y, Nakagawa H, Nukuda T, Price WS. Ionic Conduction and Ion Diffusion in Binary Room-Temperature Ionic Liquids Composed of [emim][BF4] and LiBF4. J Phys Chem B 2004;108:19527–32.

[55]   Guyomar A, Delanonoy P, Dupré N, Cerclier C, Humbert B, Bideu J. Destructuring ionic liquids in ionogels : enhanced fragility for solid devices. Phys Chem Chem Phys 2014;16:23639–45.

[56]   Gardas RL, Coutinho JAP. Extension of the Ye and Shreeve group contribution method for density estimation of ionic liquids in a wide range of temperatures and pressures. Fluid Phase Equilib 2008;263:26–32.

[57]   Ye C, Shreeve JM. Rapid and accurate estimation of densities of room-temperature ionic liquids and salts. J Phys Chem A 2007;111:1456–61.

[58]   Rennie AJR, Martins VL, Torresi RM, Hall PJ. Ionic Liquids Containing Sulfonium Cations

as Electrolytes for Electrochemical Double Layer Capacitors. J Phys Chem C 2015;119:23865–74.

[59]   Sayah S, Ghamouss F, Santos-Peña J, Tran Van F, Lemordant D. The Intriguing Properties of 1-Ethyl-3-methylimidazolium bis(fluorosulfonyl)imide Ionic Liquid. J Solution Chem 2019;48:992–1008.

[60]   Miller AA. "Free Volume" and the Viscosity of Liquid Water. J Chem Phys 1963;38:1568–71.

[61]   Lewandowski A, Świderska-Mocek A. Ionic liquids as electrolytes for Li-ion batteries. An overview of electrochemical studies. J Power Sources 2009;194:601–9.

[62]   Monteiro MJ, Camilo FF, Ribeiro MCC, Torresi RM. Ether-bond-containing ionic liquids and the relevance of the ether bond position to transport properties. J Phys Chem B 2010;114:12488–94.

[63]   McDowell MT, Lee SW, Nix WD, Cui Y. Understanding the lithiation of silicon and other alloying anodes for lithium-ion batteries. Adv Mater 2013;25:4966–85.

[64]   Botas C, Carriazo D, Zhang W, Rojo T, Singh G. Silicon-Reduced Graphene Oxide Self-Standing Composites Suitable as Binder-Free Anodes for Lithium-Ion Batteries. ACS Appl Mater Interfaces 2016;8:28800–8.

[65]   Shao D, Tang D, Mai Y, Zhang L. Nanostructured silicon/porous carbon spherical composite as a high capacity anode for Li-ion batteries. J Mater Chem A 2013;1:15068–75.

Four phosphonium-based ionic liquids. Synthesis, characterization and electrochemical performance as electrolytes for silicon anodes

Nedher Sánchez-Ramírez[a,d], Ivonne E. Monje[a], Vitor L. Martins[a], Daniel Bélanger[b], Pedro H.C. Camargo[a,c] and Roberto M. Torresi[a].

[a]*Departamento de Química Fundamental, Instituto de Química – Universidade de São Paulo, Av. Prof. Lineu Prestes 748, 05500-000, São Paulo, Brazil*

[b]*NanoQAM and Département de Chimie Université du Québec à Montréal, Case Postale 8888 Succursale Centre-Ville, Montréal, Québec, H3C 3P8, Canada*

[c]*Department of Chemistry, University of Helsinki, A.I. Virtasen Aukio 1, 00014 Helsinki, Finland*

[d]*Departamento de Ciencias, Universidad de Ingenieria y Tecnologia – UTEC, Barranco, Lima, Peru*

Figure S1: ^{1}H (a) and ^{13}C (b) NMR of *[P$_{2228}$][FSI]*.

[P$_{2228}$][FSI] Data. Elemental analysis data: Found: C; 40.9; H; 7.85; N; 3.49. Calc for: $C_{14}H_{32}PNS_2O_4F_2$: C; 40.9; H; 7.84; N; 3.40; δ_H (500 MHz; CD$_3$CN; ppm): 0.88-0.91 (3H; t; *J* = 7,5 Hz); 1.15-1.21 (9H; m); 1.27-1.35 (8H; m); 1.41-1.56 (4H; m); 2.03-2.15 (8H; m); δ^{13}C (500 MHz; CD$_3$CN; ppm): 5.80 (3C); 12.0-12.4 (3C; d; $^1J_{CP}$ = 50 Hz); 14.4; 17.8-18.2 (1C; d; $^1J_{CP}$ = 49 Hz); 21.8; 23.4; 29.5; 29.7; 31.4; 32.6 (Figures S1, supplementary information (SI)).
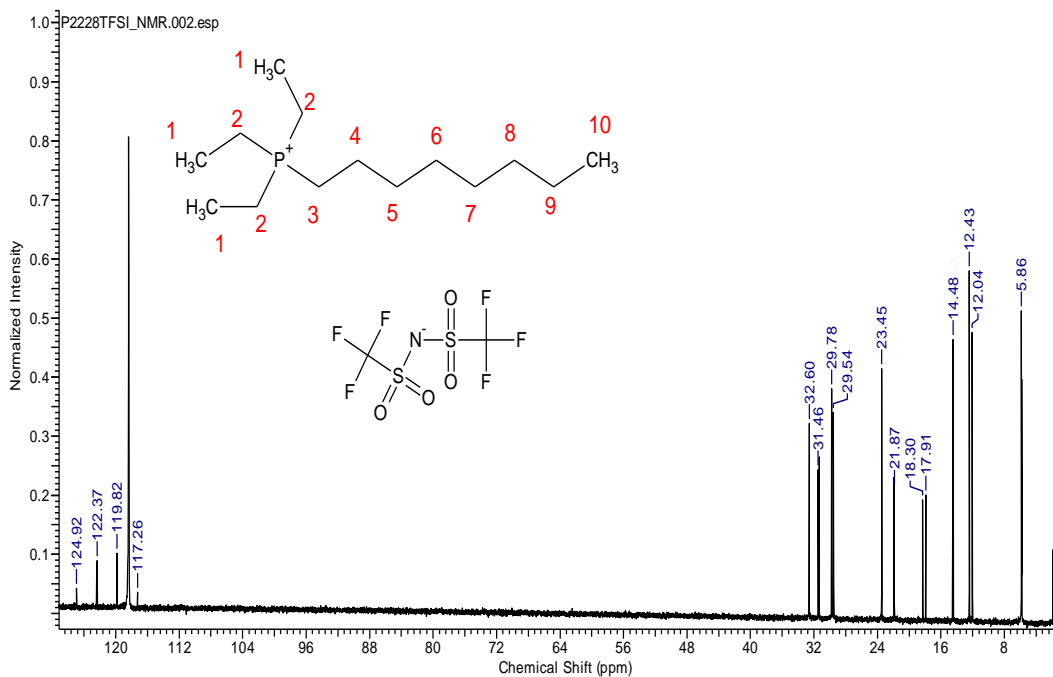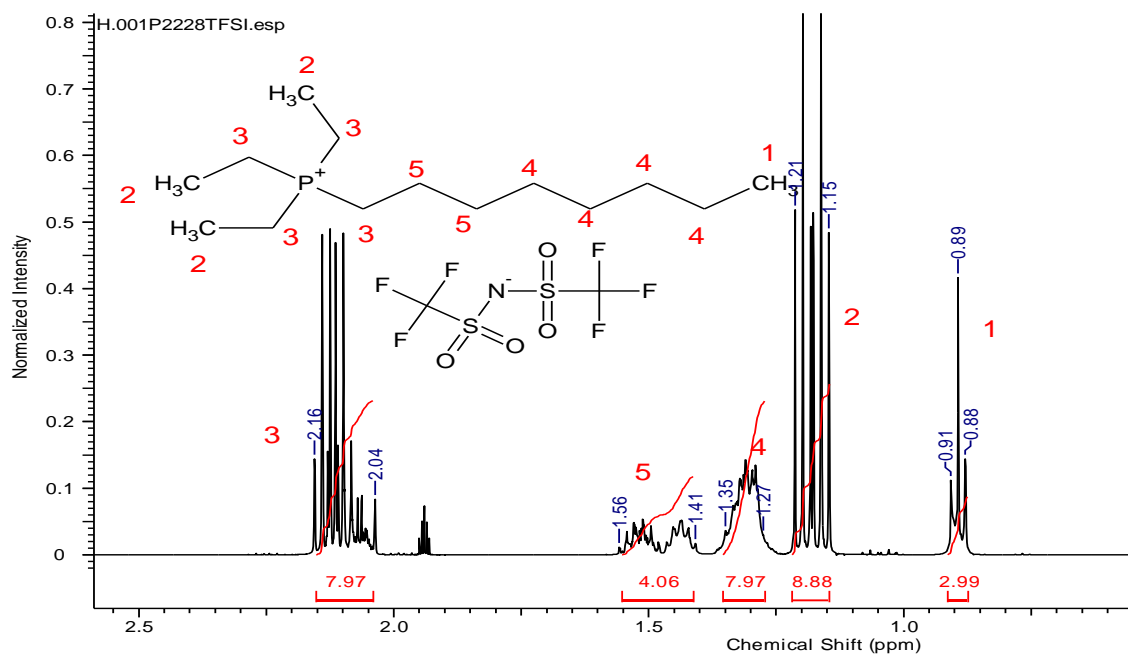
Figure S2: ^{1}H (a) and ^{13}C (b) NMR of *[P₂₂₂₈][TFSI]*.

[P₂₂₂₈][TFSI] Data. Elemental analysis data: Found: C; 37.7; H; 6.31; N; 2.77. Calc for: $C_{16}H_{32}PNS_2O_4F_6$: C; 37.6; H; 6.30; N; 2.74; δ_H (500 MHz; CD₃CN; ppm): 0.88-0.91 (3H; t; J = 7,5 Hz); 1.15-1.21 (9H; m); 1.27-1.35 (8H; m); 1.41-1.56 (4H; m); 2.04-2.16 (8H; m); $\delta^{13}C$ (500 MHz; CD₃CN; ppm): 5.86 (3C); 12.0-12.4 (3C; d; $^1J_{CP}$ = 49 Hz); 14.5; 17.9-18.3 (1C; d; $^1J_{CP}$ = 49 Hz); 21.9; 23.4; 29.5; 29.8; 31.3; 32.6; 117.3-124.9 (2C; q; $^1J_{CF}$ = 319 Hz). (Figures S2, SI)
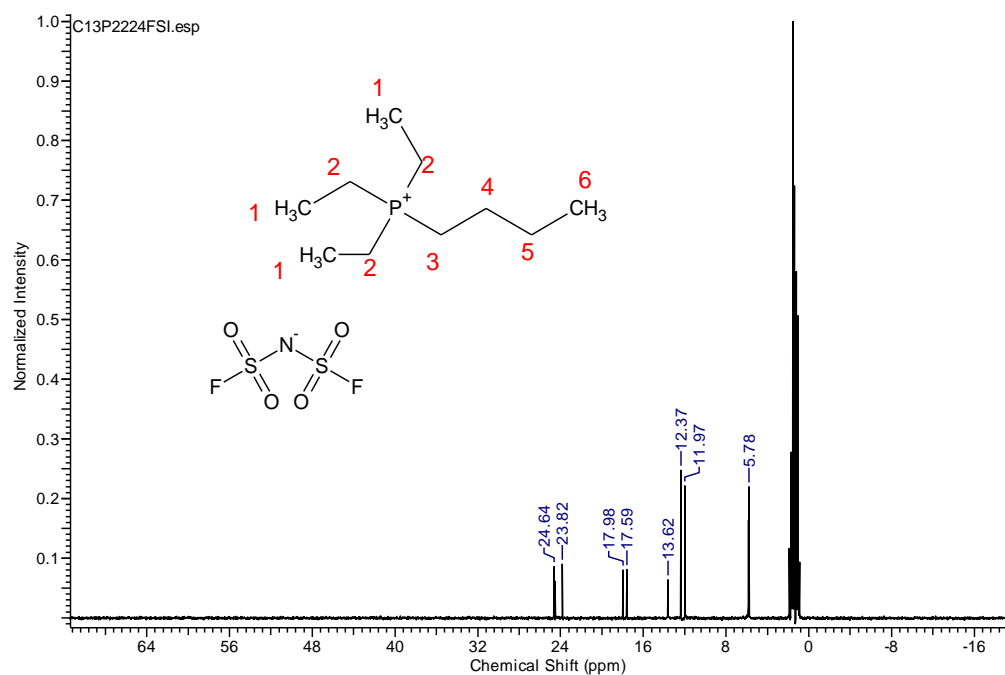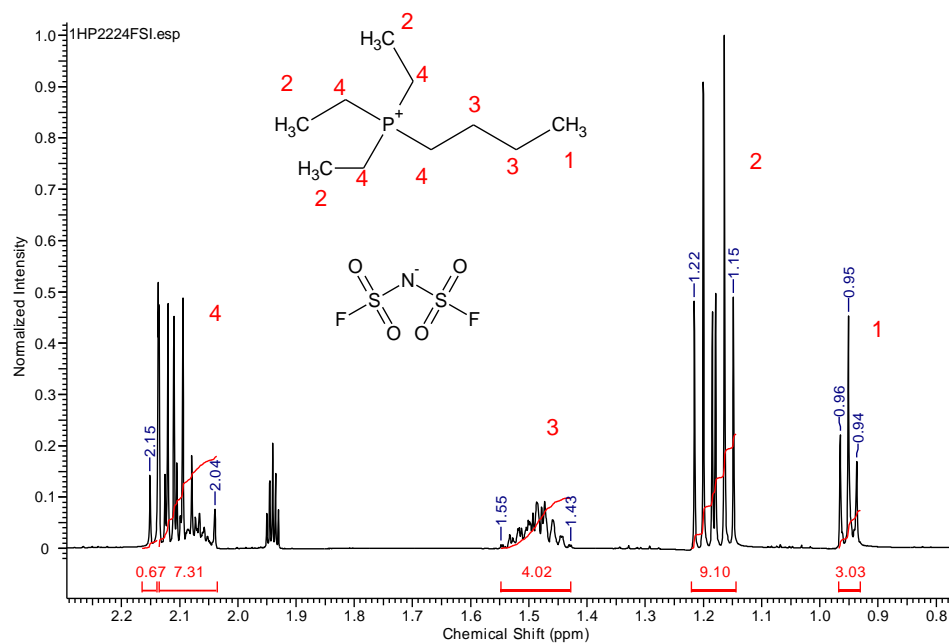
Figure S3: ^{1}H (a) and ^{13}C (b) NMR of *[P₂₂₂₄][FSI]*.

[P₂₂₂₄][FSI] Data. Elemental analysis data: Found: C; 33.9; H; 6.75; N; 3.88; Calc for: $C_{10}H_{24}F_2NO_4PS_2$: C; 33.8; H; 6.80; N; 3.94; δ_H (500 MHz; CD$_3$CN; ppm): 0.94-0.96 (3H; t; $J = 5$ Hz); 1.15-1.21 (9H; m); 1.43-1.55 (4H; m); 2.04-2.15 (8H; m); δ^{13}C (500 MHz; CD$_3$CN; ppm): 5.78 (3C); 12.0-12.4 (3C; d; $^1J_{CP}$ = 50 Hz); 13.6; 17.6-18.0 (1C; d; $^1J_{CP}$ = 49 Hz); 23.8; 24.6. (Figures S3, SI)
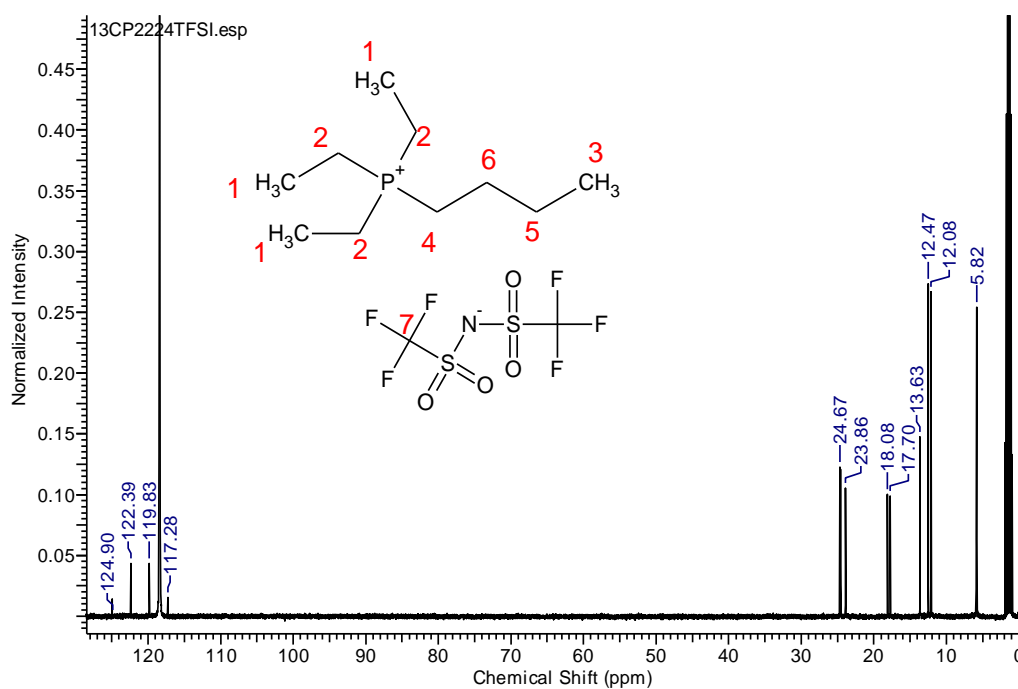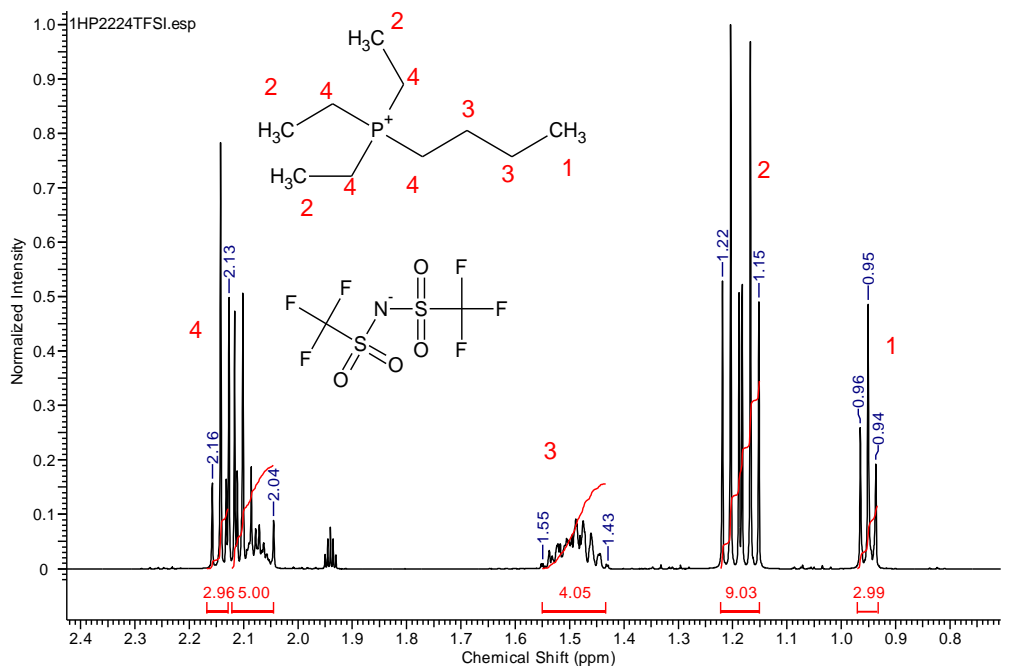
Figure S4: ^1H (a) and ^{13}C (b) NMR of *[P$_{2224}$][TFSI]*.

[P$_{2224}$][TFSI] Data. Elemental analysis data: Found: C; 30.9; H; 5.5; N; 3.03; Calc for: $C_{12}H_{24}F_6NO_4PS_2$: C; 31.6; H; 5.3; N; 3.1; δ_H (500 MHz; CD$_3$CN; ppm): 0.94-0.96 (3H; t; $J = 5$ Hz); 1.15-1.22 (9H; m); 1.43-1.55 (4H; m); 2.04-2.16 (8H; m); $\delta^{13}C$ (500 MHz; CD$_3$CN; ppm): 5.82 (3C); 12.1-12.5 (3C; d; $^1J_{CP} = 49$ Hz); 13.6; 17.7-18.1 (1C; d; $^1J_{CP} = 48$ Hz); 23.9; 24.7, 117.3-124.9 (2C; q; $^1J_{CF} = 318$ Hz) (Figures S4, SI).

Table S1. VTF parameters for viscosity

IL	η_o	B	To	D	R^2
[P$_{2224}$][FSI]	0.17091	841.1	155.4	5.411	0.999
[P$_{2224}$FSI]+ 1 M LiTFSI	0.2316	811.6	164.1	4.946	0.999
[P$_{2228}$][FSI]	0.15666	885.3	161.4	5.485	0.999
[P$_{2228}$FSI]+ 1 M LiFSI	0.2039	871.9	165.5	5.269	0.999
[P$_{2228}$][TFSI]	0.13828	828.7	175.4	4.725	0.999
[P$_{2228}$TFSI]+ 1 M LiTFSI	0.1649	837.8	192.9	4.342	0.999

Table S2. VTF parameters for conductivity.

IL	ko	B'	To'	D'	R2
[P$_{2224}$][FSI]	0.7663	825.4	137.0	6.023	0.999
[P$_{2224}$FSI]+ 1 M LiTFSI	0.9776	1072.1	117.4	9.131	0.999
[P$_{2228}$][FSI]	1.1569	1361.6	92.5	14.721	0.997
[P$_{2228}$FSI]+ 1 M LiFSI	0.6041	1049.7	132.3	7.934	0.999
[P$_{2228}$][TFSI]	1.5229	1378.1	110.8	12.436	0.999
[P$_{2228}$TFSI]+ 1 M LiTFSI	388.2462	3540.0	51.6	68.597	0.999

Table S3. Calculated and experimental density for ILs with Li$^+$ salt addition at 298 and 373 K.

IL	Temperature	$\rho_{exp.}$(g cm^{-3})	$\rho_{calc.}$(g cm^{-3})	|Error (%)|
[P$_{2228}$][TFSI]	298	1.331	1.315	1.22
	373	1.275	1.262	0.88
[P$_{2228}$][FSI]	298	1.233	1.255	1.75
	373	1.179	1.195	1.34
[P$_{2224}$][FSI]	298	1.306	1.330	1.80
	373	1.248	1.266	1.42

Table S4. Density, viscosity and ionic conductivity of neat [P$_{2224}$][FSI] in the studied temperature range.

[P$_{2224}$][FSI]					M.W. (g mol^{-1})
					355.40
T			Density	Viscosity	Conductivity
°C	K	1/K *1000	g cm^{-1}	m Pa s	mS cm^{-1}
25	298.15	3.35	1.241	61.32	4.56
27	300.15	3.33	1.240	56.58	4.86
33	306.15	3.27	1.235	45.17	5.82
39	312.15	3.20	1.231	36.62	6.89
45	318.15	3.14	1.226	30.15	8.05
51	324.15	3.08	1.222	25.10	9.30
57	330.15	3.03	1.217	21.16	10.67
63	336.15	2.97	1.213	18.03	12.13
68	341.15	2.93	1.209	15.88	
75	348.15	2.87	1.204	13.44	15.37
82	355.15	2.82	1.199	11.50	
88	361.15	2.77	1.195	10.13	
100	373.15	2.68	1.187	8.024	

Table S5. Density, viscosity and ionic conductivity of 1M of LiFSI in [P$_{2224}$][FSI] in the studied temperature range.

[P$_{2224}$][FSI] + 1M LiFSI					
T			Density	Viscosity	Conductivity
°C	K	1/K *1000	g cm^{-1}	m Pa s	mS cm^{-1}
25	298.15	3.35	1.306	97.27	**2.52**
27	300.15	3.33	1.304	89.24	**2.80**
33	306.15	3.27	1.300	69.87	**3.44**
39	312.15	3.20	1.295	55.69	**3.95**
45	318.15	3.14	1.290	45.11	**4.61**
51	324.15	3.08	1.286	37.08	**5.40**
57	330.15	3.03	1.281	30.87	**6.45**
63	336.15	2.97	1.276	26.02	**7.24**
68	341.15	2.93	1.272	22.75	
75	348.15	2.87	1.267	19.06	**9.37**
82	355.15	2.82	1.262	16.16	
88	361.15	2.77	1.257	14.15	
100	373.15	2.68	1.248	11.07	

Table S6. Density, viscosity and ionic conductivity of neat [P$_{2228}$][FSI] in the studied temperature range.

[P$_{2228}$][FSI]					M.W. (g mol^{-1})
					411.50
T			Density	Viscosity	Conductivity
°C	K	1/K *1000	g cm^{-1}	m Pa s	mS cm^{-1}
25	298.15	3.35	1.165	99.46	1.50
27	300.15	3.33	1.164	90.95	1.61
33	306.15	3.27	1.159	70.48	1.99
39	312.15	3.20	1.155	55.59	2.40
45	318.15	3.14	1.151	44.57	2.84
51	324.15	3.08	1.147	36.26	3.28
57	330.15	3.03	1.143	29.90	3.72
63	336.15	2.97	1.139	24.95	4.21
68	341.15	2.93	1.135	21.63	
75	348.15	2.87	1.130	17.94	5.68
82	355.15	2.82	1.125	15.06	
88	361.15	2.77	1.121	13.07	
100	373.15	2.68	1.113	10.08	

Table S7. Density, viscosity and ionic conductivity of 1M of LiFSI in [P$_{2228}$][FSI] in the studied temperature range.

[P$_{2228}$][FSI] + 1M					
T			Density	Viscosity	Conductivity
°C	K	1/K *1000	g cm^{-1}	m Pa s	mS cm^{-1}
25	298.15	3.35	1.233	142.2	1.05
27	300.15	3.33	1.232	129.8	1.17
33	306.15	3.27	1.228	99.50	1.48
39	312.15	3.20	1.224	77.74	1.88
45	318.15	3.14	1.219	61.77	1.94
51	324.15	3.08	1.215	49.92	2.51
57	330.15	3.03	1.211	40.87	3.07
63	336.15	2.97	1.207	33.90	3.54
68	341.15	2.93	1.203	29.27	
75	348.15	2.87	1.198	24.12	4.65
82	355.15	2.82	1.192	20.14	
88	361.15	2.77	1.188	17.42	
100	373.15	2.68	1.179	13.35	

Table S8. Density, viscosity and ionic conductivity of neat [P$_{2228}$][TFSI] in the studied temperature range.

[P$_{2228}$][TFSI]					M.W. (g mol^{-1}) 511.50
T			**Density**	**Viscosity**	**Conductivity**
°C	**K**	**1/K *1000**	**g cm^{-1}**	**m Pa s**	**mS cm^{-1}**
25	298.15	3.35	1.245	115.4	0.972
27	300.15	3.33	1.243	104.0	1.05
33	306.15	3.27	1.238	77.55	1.32
39	312.15	3.20	1.233	59.15	1.62
45	318.15	3.14	1.228	46.06	1.98
51	324.15	3.08	1.224	36.55	2.38
57	330.15	3.03	1.219	29.48	2.84
63	336.15	2.97	1.214	24.14	3.37
68	341.15	2.93	1.210	20.63	
75	348.15	2.87	1.205	16.77	4.58
82	355.15	2.82	1.199	13.86	
88	361.15	2.77	1.194	11.88	
100	373.15	2.68	1.185	8.980	

Table S9. Density, viscosity and ionic conductivity of 1M of LiFSI in [P$_{2228}$][TFSI] in the studied temperature range.

[P$_{2228}$][TFSI] + 1 M					
T			**Density**	**Viscosity**	**Conductivity**
°C	**K**	**1/K *1000**	**g cm^{-1}**	**m Pa s**	**mS cm^{-1}**
25	298.15	3.35	1.331	443.4	0.224
27	300.15	3.33	1.329	386.5	0.257
33	306.15	3.27	1.323	262.6	0.367
39	312.15	3.20	1.318	184.2	0.566
45	318.15	3.14	1.313	132.9	0.610
51	324.15	3.08	1.308	98.43	0.819
57	330.15	3.03	1.302	74.62	1.13
63	336.15	2.97	1.297	57.74	1.63
68	341.15	2.93	1.293	47.31	
75	348.15	2.87	1.286	36.53	2.52
82	355.15	2.82	1.280	28.77	
88	361.15	2.77	1.275	23.77	
100	373.15	2.68	1.264	16.84	

Table S10. Density, viscosity and ionic conductivity of neat EC/DEC in the studied temperature range.

EC/DEC					M.M.of the mixture 98.78
T			Density	Viscosity	Conductivity
°C	K	1/K *1000	g cm^{-1}	m Pa s	mS cm^{-1}
25	298.15	3.35	1.134	1.573	0.498
27	300.15	3.33	1.132	1.528	0.515
33	306.15	3.27	1.125	1.400	0.558
39	312.15	3.20	1.119	1.287	0.606
45	318.15	3.14	1.112	1.189	0.661
51	324.15	3.08	1.105	1.105	0.730
57	330.15	3.03	1.099	1.032	0.814
63	336.15	2.97	1.092	0.9678	0.917
68	341.15	2.93	1.086	0.8882	
75	348.15	2.87	1.079	0.8541	1.13
82	355.15	2.82	1.070	0.7659	
88	361.15	2.77	1.064	0.7328	